eprints@whiterose.ac.uk
https://eprints.whiterose.ac.uk/

Lead Sulfide Scaling in Multiphase Systems and Co-precipitation in the Presence of Calcium Carbonate

William Keogh*[†], Anne Neville[†], Qingxia Liu[‡], Liyuan Feng[‡], Chenxin Jin[‡], Frank Møller Nielsen[§], John Helge Olsen[§], Salima Baraka-Lokmane[‖], Jon Arne Ellingsen[⊥], Stuart Micklethwaite[¶], David Harbottle[¶], Thibaut Charpentier[¶]

[†] Institute of Functional Surfaces (iFS), University of Leeds, Leeds, LS2 9JT, England

[‡] Department of Chemical and Materials Engineering, University of Alberta, Edmonton, Alberta, T6G 1H9, Canada

[§] Equinor ASA, 5020, Bergen, Norway

[‖] TOTAL, 64000, Pau, France

[⊥] Conoco Phillips, 4056, Stavanger, Norway

[¶] School of Chemical and Process Engineering, University of Leeds, Leeds, LS2 9JT, England

Abstract

Undesirable precipitation of sulfide scales during hydrocarbon production, typically in sour, high temperature and high pressure systems, add an additional level of complexity to both predicting and controlling of inorganic mineral deposition. The fundamental mechanism promoting nucleation and deposition of extremely insoluble mineral scale species such as lead sulfide (PbS) in liquid-liquid systems follows spontaneous nucleation of metal sulfide nanoparticles, and their

assembly at oil-water interfaces, before oil droplets impact on surfaces leading to nanoparticle transfer and deposition. Conversely, common mineral scales such as calcium carbonate ($CaCO_3$) possesses a higher degree of solubility, generally resulting in heterogeneous crystallization directly upon surfaces. Co-precipitation of sulfide and carbonate species is frequently encountered during production, yet the literature addressing the topic is scarce. This is the first study assessing the influence of a light oil phase on PbS-$CaCO_3$ co-precipitation behavior.

This study showed that the depositional behavior of PbS nanoparticles precipitated in a simple liquid-liquid system can be accurately predicted, based on particle wettability, oil to water ratio and the surface energy and wettability of the contact surface where nanoparticle accumulation occurs. Analysis of co-precipitation between PbS and $CaCO_3$ highlighted differences in the precipitation mechanism between the two minerals. PbS agglomerates assembled at the oil-water interface acting as seeding points for the nucleation and growth of calcite, resulting in a strongly adsorbed PbS/$CaCO_3$ complex that resulted in significant deposition on hydrophilic surfaces.

1. Introduction

Inorganic mineral fouling in producing oilfields has resulted in millions of dollars of operating expenditure year on year since the inception of offshore oil and gas drilling, where scale deposition in tubing, flowlines and downhole equipment leads to significant production downtime.[1] The technological challenge of producing from high temperature/high pressure (HT/HP) wells coupled with the increasing risk of reservoir souring brings with it additional complexities, whereby increased corrosion rates and the deposition of sulfide based scales such as lead sulfide (PbS), zinc sulfide (ZnS) and iron sulfide (FeS) can cause production issues and well failure.[2] PbS scale deposits have become a concern in several North Sea oil and gas fields, rich in both evolved hydrogen sulfide (H_2S) gas and formation metal ions.[3] Though depositional behavior can be largely anticipated in simple multiphase laboratory tests where PbS is the only salt formed,[4] an abundance of mineral forming ions both in formation waters and injected seawater in the reservoir leads to complex association, with the effects of co-precipitation, inhibition by divalent cations and constantly changing mineral solubility leading to unpredictable scaling scenarios.[5, 6, 7, 8]

$CaCO_3$ fouling is endemic in oilfield systems, as produced water containing both bicarbonate (HCO_3^-) and calcium (Ca^{2+}) ions is prone to form precipitates simply as a result of pressure changes during production and seawater injection. The release of carbon dioxide (CO_2) gas from the aqueous phase prompts the evolution of carbonate (CO_3^{2-}), resulting in a rise in pH and consequent precipitation.[2] The additional reduction of $CaCO_3$ solubility with increased temperature dictates that precipitation can occur anywhere from the wellbore to the topside, with case studies showing precipitation of PbS and $CaCO_3$ species both near the wellbore and higher up the production tubing.[9, 10] PbS precipitation tendency is significantly influenced by temperature, salinity and pH, and as such is analyzed on a well-by-well basis through both modelling techniques and fouling analysis after equipment recovery.[10] The likelihood of co-precipitation occurring is high, where

the spontaneous precipitation of barely soluble PbS towards the wellhead occurs in tandem with $CaCO_3$ crystallization.

Whilst numerous studies have considered the fouling behavior of sulfide mineral scales in single phase systems,[11, 12] the significance of the presence of a light oil phase with regards to deposition of various salts is considerable.[4, 13] In a multiphase system where PbS is spontaneously nucleated within the bulk homogeneous phase, the degree of fouling deposition can be reasonably predicted based on the wettability of the substrate.[13] Heterogenous nucleation however occurs directly onto surfaces that results in the compromising of a substrate's anti-fouling attributes, ultimately changing the wettability. Consequently, the two key elements for determining the deposition of bulk precipitated particles in turbulent multiphase systems include; i) particle or agglomerate wetting at the oil-water (o-w) interface and the formation of a Pickering emulsions; and ii) the hydrophobicity of the substrate.[13]

When immiscible crude oil and water are simultaneously present within a producing system, particles or droplets of one phase will become dispersed within the continuous phase of the other, dependent on the o:w ratio. The natural evolution of a producing well dictates that there will be an inevitable increase in water-cut throughout its lifetime and as such, the potential for inversion of any solid stabilized water-in-oil (w/o) emulsion to an o/w state.[14] The position, packing fraction and wettability of various colloid species stabilized across the o-w interface determines the oil:water (o:w) ratio at which emulsion inversion occurs.[15]

This study aims to characterize the fundamental behavior of PbS particles at oil-water interfaces and solid surfaces and observe the influence of commonly occurring calcium carbonate ($CaCO_3$) scale upon co-precipitation with PbS.

2. Background

When precipitated at ionic concentrations expected in typical sour oilfield brines (55 ppm H_2S; 50 ppm Pb^{2+}), the low solubility of PbS under ambient conditions ($K_{sp} = 3 \times 10^{-28}$) and hence high thermodynamic driving force for crystallization results in spontaneous homogeneous nucleation of cubic nanoparticles and limited crystal growth.[11, 16] In oilfield conditions however, the typically low solubility of PbS is significantly increased by high free chloride ion concentration, temperature and low pH, that can result in precipitation in the production tubing as opposed to the wellbore.[10, 17, 18] PbS nanocrystals, typically around 30 - 60 nm in diameter after precipitation, are prone to agglomerate as a consequence of attractive van-der-Waals (vdW) forces coupled with limited electrostatic repulsion, where the zeta potential (ζ) of nanoparticles at pH 5.2 was measured to be -9 mV in 0.5 M KCl solutions.[19] $CaCO_3$ has comparably high solubility ($K_{sp} = 3.36 \times 10^{-9}$) at ambient temperature, resulting in lower levels of supersaturation when contrasted with metal sulfides that leads to heterogeneous crystallization induced by surfaces, impurities and phase boundaries.[20-23] The extensive growth of calcite may be explained by the presence of many small crystallites on the growing face, exhibiting rough surfaces with a multitude of kink-and-step sites.[24]

Mineral surfaces are usually heterogeneous due to the existence of impurities/functional groups on the surface, crystal orientation and hydrophilic/hydrophobic sites on the surface, therefore a single value for surface energy is not representative of the whole surface. Sulfide minerals have a low degree of surface polarity and hydrophobic characteristics, potentially as a result of surface oxidation and hydrolysis. Whilst sessile drop measurements provided a crude measure of PbS wettability, the heterogeneous distribution of hydrophobic sites upon the PbS [001] crystal plane results in the characterization of PbS mineral throughout this work as 'partially hydrophobic'.[25]

Irreversible attachment of partially hydrophobic PbS particles occurs at the o-w interface, where the free energy of desorption for a 50 nm radius PbS particle of at an oil-water interface ($\gamma_{ow} = 50$ mN m^{-1}), exhibiting a water contact angle (θ_w) of 49°, results in a free energy of $\Delta G_w = 1.3$ x 10^{-16} J. This is much larger than the thermal energy K_bT (5×10^{-21} J at 95° C), demonstrating the interfacial stability of the nanoparticles even at high temperatures.[15, 26, 27] Mobility of particle-stabilized droplets largely occurs via mechanical means, whereby particle stabilized droplets impact against surfaces within a high-energy turbulent o-w multiphase system and either rupture or adhere.[13] Rupture of an oil or water droplet (dependent on emulsion type) after impacting a substrate can result in the deposition and adhesion of particles that previously contributed to droplet stabilization.[4, 28, 29] The adhesive strength of particles once deposited has been shown to depend on the particle size and surface energies of the two interacting species.[30, 31]

Whilst not typically observed in co-precipitation of common scaling species e.g. calcium carbonate and sulfate,[32, 33] the formation of crystal complexes and films as a consequence of occlusion co-precipitation is well documented, occurring when an impurity is trapped centrally inside of a growing crystal.[34-36] Such methods are implemented widely in industry, from remediation of gold (Au) and silver (Ag) nanoparticle contaminants within water systems through co-precipitation with $CaCO_3$,[37] to PbS nanoparticles functioning as nucleation sites to promote the formation of perovskite lattice structures to improve performance in solar cells.[38]

3. Materials and Methods

Building on previous work,[4, 13] the emulsion stabilizing characteristics and depositional mechanisms of PbS precipitated in multiphase systems were scrutinized. Sessile drop measurements determined wetting behavior of galena (PbS) in order to explain particle arrangement at the o-w interface in conjunction with cryo-SEM analysis. Co-crystallization and fouling of PbS with $CaCO_3$ simulated a system representative of the mineral scales produced and deposited in a number of sour oilfield wells.[39] Cryo-SEM analysis employed energy dispersive x-ray (EDX) and backscattered electron (BSE) detection methods, enabling increased visualization of particle arrangement at the o-w interface and the nature of incorporation. X-ray diffraction (XRD) confirmed the formation and presence of PbS and $CaCO_3$ species from the complex brine.

3.1. Scaling experiments

Figure 1 illustrates the scaling apparatus used, whereby the methodology used followed that of Keogh et al.[13] for simple scaling tests. Four cylindrical anti-fouling samples (3.77 cm^2 each) were rotated at 400 RPM to propagate turbulence at the interface, where the Reynolds number (*Re*) was calculated to be 3374. A bladed impeller in solution prompted the formation of an emulsion when both oil and water were present in the vessel. Gas in a blend of 1% H_2S/99% N_2 was introduced into the air phase of the airtight reaction vessel at a constant pressure of 1.1-1.2 bar (absolute), controlled via a regulator connected to a pressurized cylinder.
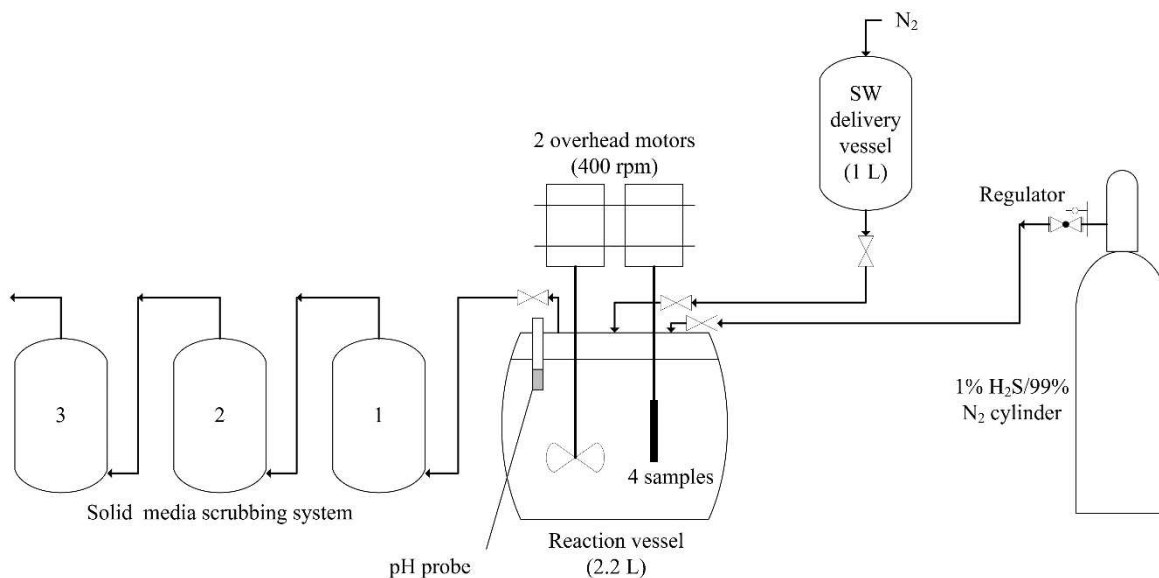
Figure 1 Scaling rig with H$_2$S injection capability and seawater (SW) delivery vessel

Nitrogen (N$_2$) sparging of brines was performed for 1 h before the experiment to ensure an anoxic environment representative of near-wellbore conditions, limiting the formation of sulfates. H$_2$S was introduced into the airspace of the reaction vessel in a 1% H$_2$S/99% N$_2$ blend for 1 h. The brine composition and initial saturation ratio (SR$_{initial}$) of solutions are shown in Table 1, where SR$_{initial}$ for PbS was calculated from the ion activity product (IAP) and solubility product (K$_{sp}$).[40] [41] [42] The effect of decreased pH and Cl$^-$ presence was taken into consideration during calculations for PbS solubility.[18]

Brines were prepared in Milli-Q water with a resistivity 18.2 MΩ·cm, with 100 mL of 5 M acetic acid buffer introduced in order to stabilize the solution pH at 5.2. Acetate buffer solution compositions and mixing ratios can be seen in Supporting Information Table S1 and Table S2 respectively.

Kerosene (C_{10} - C_{16}, ACS reagent grade, Fisher Scientific), as the light oil phase, was added in o:w ratios of 5:95 and 80:20 for tests in o/w and w/o emulsion forming systems respectively for PbS systems. Table 1 shows the ionic concentration of brines used in simple PbS scaling systems.

Table 1 PbS forming brine concentration and $SR_{initial}$

Ion	Ionic concentration (mg/L)		$SR_{initial}$
	Formation water	*H_2S injection*	
Pb^{2+}	1000	-	
K^+	19405	-	PbS = 1.7 x 10^{19}
Cl^-	17938	-	
HS^-	-	30 (at equilibrium)	

For co-precipitation experiments, two de-aerated incompatible brines were introduced using the seawater (SW) delivery vessel and injected through overpressure into the reaction vessel immediately before the H_2S blend stream was activated, initiating the test. Brine composition and $SR_{initial}$ are available in Table 2, where the two dominant precipitating species were PbS and $CaCO_3$, with $SR_{initial}$ calculated using IAP/K_{sp} values and Multiscale^{TM} software respectively, where PbS solubility was adjusted for a high salinity brine and pH 5.2 solution.[18] Kerosene was added in o:w ratios of 5:95 and 60:40 to prompt formation of o/w and w/o emulsions respectively.

Table 2 PbS and $CaCO_3$ forming brine concentration and $SR_{initial}$

Ion	Ionic concentration (mg/L)		$SR_{initial}$
	Formation water	*Sea water*	
Na^+	10000	11744	PbS = 1.3 x 10^{17} CaCO₃ = 76
Ca^{2+}	8000	-	
K^+	468	-	
Mg^{2+}	1118	-	
Pb^{2+}	100		
HCO_3^-	-	7002	
HS^-	-	30 (at equilibrium)	
Cl^-	38196		

Post-experiment, the H_2S/N_2 stream was stopped and the system flushed with pure N_2 to fully remove H_2S within the reaction vessel and feed lines into the scrubbers. Sample coupons were then removed and dried under a N_2 stream before weighing.

Additional pre-precipitation experiments were performed whereby pre-precipitated PbS nanoparticles were introduced into the formation water (FW) brine prior to the experiment. A H_2S blend was not introduced into the reaction vessel, as the aim of the experiment was to observe if PbS acted as the seeding point for calcite growth.

3.2. Anti-fouling surfaces

A number of anti-fouling coatings with contrasting physiochemical characteristics were used for anti-fouling experiments. The wettability of anti-scaling surfaces, particularly in multiphase conditions, has been shown to be of importance with regard to the extent of inorganic scale

deposition.[4] Table 3 lists the name and type of coatings evaluated, as well as wettability and roughness (R_a) values. Coatings F1 and F2 are classified as hydrophobic (water contact angle > 90°), whilst REF and DLC are classified as hydrophilic (water contact angle < 90°).

Table 3 Anti-fouling coatings

Coating	Coating type	Water contact angle (°)	R_a (µm)	
REF	UNS N07718 (none)	71	0.01	
DLC	Diamond-like carbon	68	0.01	
F1	Fluoro-polymer	101	3.62	
F2		103	0.93	

3.3. Pickering emulsion characterization

Post-experiment, Pickering emulsions were siphoned and collected in 20 mL vials, where a proportion of oil and water was also collected from the reaction vessel. Starting with approximately 5 mL of recovered brine containing 1 mL of particle-stabilized o/w emulsion and 1 mL of light phase oil, 0.5 mL of oil was added drop-wise. The vial was shaken and agitated, with an image taken after each oil addition until the point of emulsion inversion from o/w to w/o was observed.[43]

To analyze the stabilizing nanoparticles, optical and cryo-SEM microscopy were performed, the latter on a Hitachi SU8230 SEM (Tokyo, Japan). Optical microscopy allowed visualization of the

oil droplet polydispersity and particle agglomerate arrangement at the interface, whilst cryo-SEM allowed more detailed analysis of PbS nanoparticle distribution and visualization of wetting at the emulsion interface, with BSE techniques able to distinguish and highlight PbS arrangement at liquid interfaces and after co-precipitation when PbS agglomerates were occluded with $CaCO_3$ crystals.

3.4. PbS wettability

A sealed quartz cell and an inverted sessile drop set up with an oil droplet injected into an aqueous electrolyte phase was used to study the oil droplet contact angle on a galena surface, shown in the Supporting Information Figure S1. Galena (Ward's Science, NY, USA) was cleaved along the [001] plane and polished until smooth and flat along the face before being set within resin. To ensure a reduction in oxidation product formation (e.g. PbO),[44] the sample was polished using fine grade silicon carbide sandpaper, rinsed and N_2 dried before being placed immediately within the cell containing N_2 sparged 0.5 M KCl solution (Milli-Q water). The electrolyte solution pH was adjusted to 5.2, corresponding to pH used in scaling experiments and representative of sour oilfield brines, resulting in a galena surface charge of approximately -9 mV.[19] For each measurement, oil droplet contact angles at five different positions on the galena substrate was recorded.

3.5. X-ray diffraction (XRD)

XRD analysis using a Bruker D8 X-Ray Diffractometer allowed identification of the precipitated species in the collected post-experiment PbS and PbS/CaCO₃ Pickering emulsions. Patterns were recorded in the 2θ range between 20-90° with a step size of 0.033°/s, resulting in a 38 min runtime.

3.6. Scale deposition on anti-fouling surfaces

The degree of scale deposition upon anti-fouling surfaces post-experiment was determined by gravimetry. A scanning electron microscopy (Carl Zeiss EVO MA15 SEM (Jena, Germany)) with energy dispersive x-ray (EDX) analysis was used to highlight different elements in the deposit. The relationship between the water contact angle of the substrate and mass gain was plotted to examine the correlation between coating wettability and the amount of scale deposited in turbulent multiphase systems.

4. Results and Discussion

4.1. Emulsion characterization

4.1.1. Emulsion inversion

The point at which PbS-stabilized emulsions invert can be observed in Figure 2a, with an o/w emulsion formed above the aqueous phase when the oil volume fraction was < 0.75. Increasing the oil volume fraction > 0.75 resulted in a sudden inversion of the continuous phase from water to oil, forming a w/o emulsion. Binks and Lumsdom[15] showed that as the volume fraction of the disperse phase is increased, droplets not only become enlarged but are deformed as they are forced into closer proximity, flocculating and ripening as swelling of drops results in insufficient PbS packing fraction at o-w droplet interfaces that eventually results in coalescence. Catastrophic phase inversion then occurs after shifting of the system to its lowest energy state. Due to the partially hydrophobic nature of PbS particles, o/w emulsions are generally favored, hence the high oil fraction required to induce inversion to a low stability w/o emulsion.[45]

The point at which emulsion inversion occurs for a complex PbS/CaCO$_3$ system can be observed in Figure 2b, whereby an o/w emulsion formed above the aqueous phase when oil volume fraction

was less than 0.5. Increasing of the dispersed oil phase volume fraction to over 0.5 resulted in a catastrophic inversion, similar to that observed in PbS stabilized systems.[15]
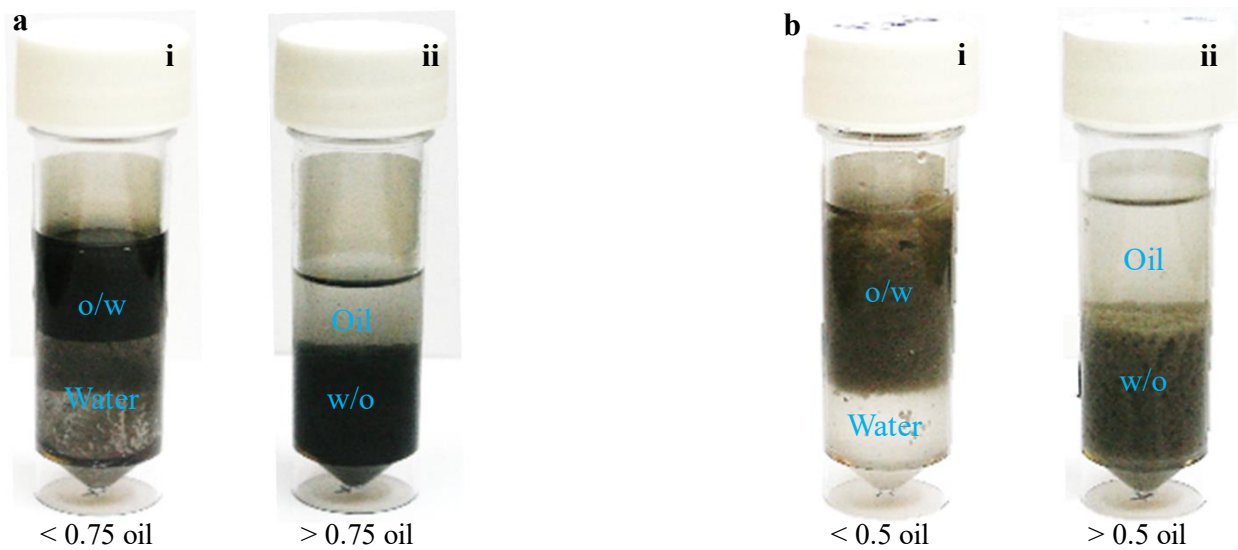
Figure 2 a) PbS system – i) o/w emulsion at < 0.75 oil phase fraction; ii) w/o emulsion at > 0.75 oil phase fraction; b) PbS/CaCO$_3$ system – i) o/w emulsion at < 0.5 oil phase fraction; ii) w/o emulsion at > 0.5 oil phase fraction

An optical microscope image of an oil droplet stabilized by PbS within an o/w emulsion can be seen in Figure 3a. At 1000 mg/L Pb^{2+} and oil phase volume fraction of approximately 0.3, the emulsion is relatively polydisperse, with oil droplet size ranging from 0.2 - 1 mm. PbS agglomerates were shown to range from 0.5 – 3 µm in diameter, and here are closely packed at the spherical interface (Figure 3b).
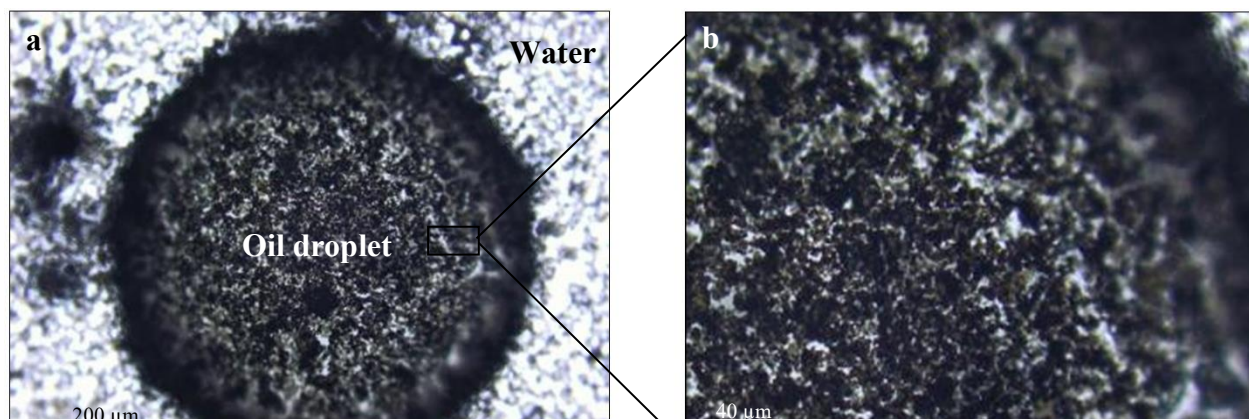
Figure 3 Optical microscope images of PbS stabilised oil droplet

Figure 4 shows optical microscope images of an oil droplet stabilized by PbS and $CaCO_3$ within an o/w emulsion, from water chemistries described in Table 2. The emulsion at the brine concentration used was relatively polydisperse, with oil droplet size ranging from 0.2-1 mm. Images show clearly PbS agglomerates as black dots up to 5 µm in diameter embedded centrally within flower-like calcite structures to form $PbS/CaCO_3$ complexes around 30-80 µm in diameter.
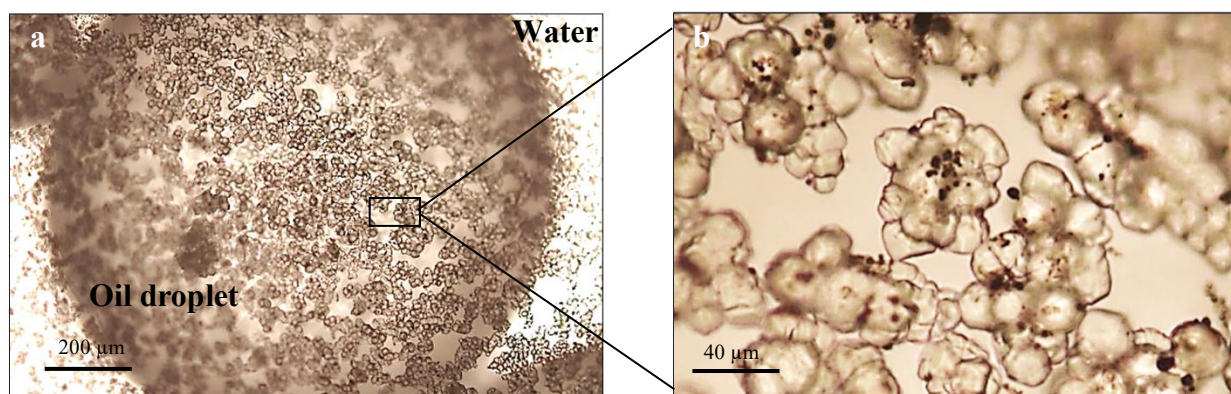
Figure 4 Optical microscope images of $PbS/CaCO_3$ stabilized oil droplet

PbS particle arrangement at the o-w interface plays an important role in emulsion stabilization, preventing the flocculation, ripening and coalescence of droplets due to high PbS packing fraction and subsequent particle jamming.[46] From comparison of oil droplet particle packing fraction in both PbS and $PbS/CaCO_3$ systems from Figure 3 and Figure 4 respectively, it can be inferred that in PbS systems, the nature of the particle/agglomerate arrangement results in a higher packing fraction of adsorbed scale at the o-w interface. PbS and $PbS/CaCO_3$ coated droplets show > 90%

and ~ 60% coverage respectively. In PbS/CaCO$_3$ systems this likely results in higher flocculation and coalescence due to the ability of oil droplets to form a bridge and ultimately coalesce at lower oil phase fractions.[47]

4.1.2. Particle arrangement at o-w interface
4.1.2.1. PbS

Optical and cryo-SEM microscopy of the o/w emulsion allowed further scrutiny of PbS nanoparticle arrangement at the oil droplet interface within an o/w emulsion. Keogh et al.[13] showed through optical microscope imaging that an oil droplet can be stabilized by cocooning of PbS particle agglomerates within the emulsion. At 1000 mg/L Pb^{2+} and oil volume fraction of approximately 0.3, the emulsion was relatively polydisperse, with oil droplet size ranging from 0.2-1 mm.

Cryo-SEM imaging (Figure 5) displays an oil droplet encased and stabilized by a thin layer of PbS nanoparticles, highlighted as white dots through the use of BSE. EDX analysis further confirmed the role of PbS in stabilization of the oil droplet (Figure 6).
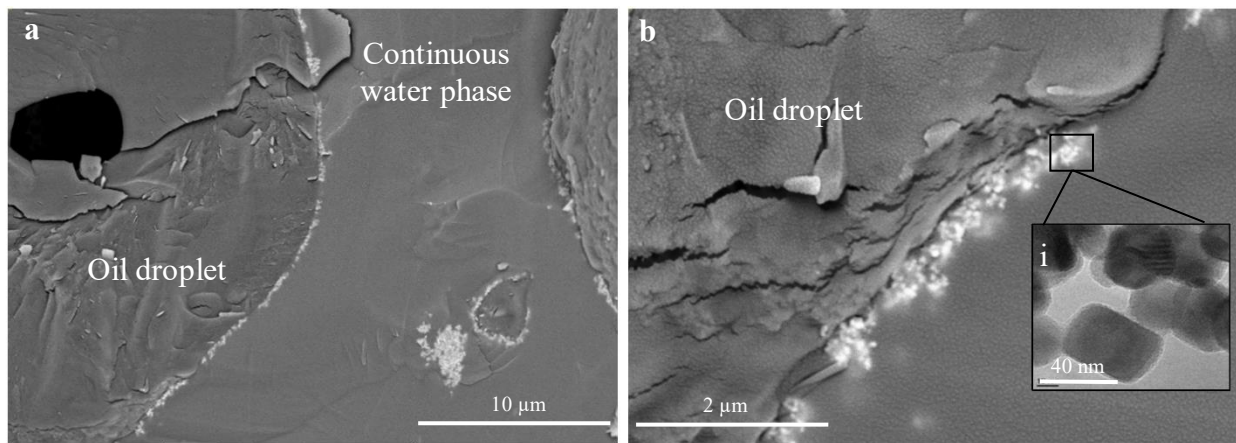
Figure 5 a & b) Cryo-SEM of oil droplet with PbS nanoparticles at o-w interface within a Pickering emulsion; b$_i$) TEM image of individual PbS nanoparticles

| Carbon (C) | Sulphur (S) | Lead (Pb) |
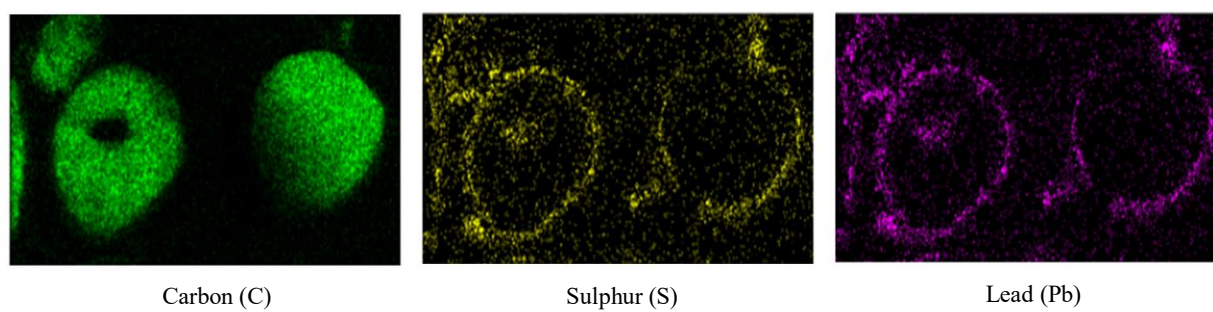
Figure 6 EDX of cryo-SEM oil droplet displaying Pb and S as PbS agglomerates at o-w interface

PbS particle arrangement can be seen in greater detail in Figure 5b, where it was revealed self-assembly of PbS agglomerates 6-10 nanoparticles deep form a network contained within the aqueous phase at the o-w interface. Transmission electron microscopy (TEM) embedded in the same image illustrates the appearance of the stabilizing PbS particles.[13]

Assembly of PbS nanoparticles in the aqueous phase at the o-w interface could be explained by their wetting properties, with attachment to the interface rather than the bulk phase driven by their partial hydrophobicity. Oil contact angle on unoxidized galena within an aqueous medium can be seen in Supporting Information Figure S2, where three-phase contact (TPC) angle at a galena-oil-water junction was $132.1 \pm 0.8°$, and $48.8 \pm 1.3°$ for a galena-water-air system.

4.1.2.2. PbS/CaCO₃

From cryo-SEM imaging (Figure 7), a semi-hemispherical indent from which an oil droplet from an o/w emulsion was dislodged after freezing was investigated. PbS/calcite complexes were arranged along the droplet oil-water interface, with BSE revealing occluded PbS agglomerates acting as the centralized nucleation point for propagating calcite crystals. EDX (Figure 8) confirmed that PbS agglomerates are incorporated into the calcite structure, with XRD analysis of the dried emulsion showing that PbS and $CaCO_3$ were the only species formed (Figure S3, Supporting Information).
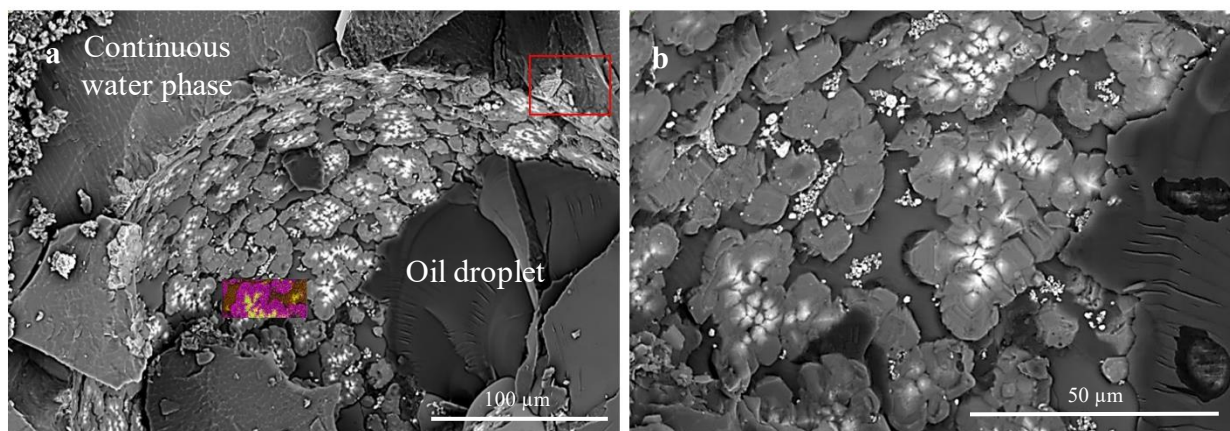
Figure 7 Cryo-SEM of oil droplet stabilised by PbS/CaCO₃ complexes

| Calcium (Ca) | Lead (Pb) | Sulphur (S) |
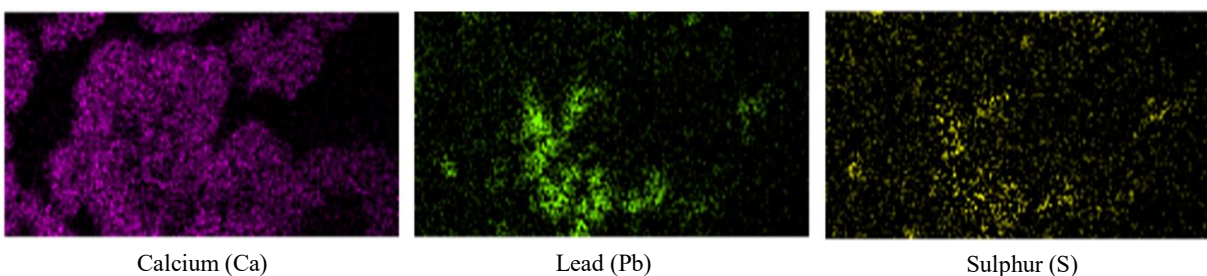
Figure 8 EDX of complex showing PbS agglomerates occluded within calcite (from Figure 7a)

Further magnification at the o-w interface (Figure 7b) showed the pyramidal structure of calcite growing outward from PbS agglomerates, known as 'hopper growth'.[48] Loose PbS agglomerates were also present at the interface that have not acted as seeding points for calcite crystallization, indicating that self-assembly had occurred at the interface prior to calcite growth. The area highlighted by the red box shows calcite that has grown at the o - w interface, extending around 20 μm and into the aqueous phase where $CaCO_3$ forming ions are available. Conversely, the PbS/$CaCO_3$ complex extends only 2 - 3 μm into the oil phase, suggesting that the free energy required for desorption from the interface is lower than that of pure PbS due to hydrophilic properties of calcite.

Calcite crystals are typically defined by a perfect rhombohedral shape with a dominant [104] face.[49] The transition between rhombohedral and hopper growth occurs at supersaturation where the growth rate of the rhombohedral crystal reaches a maximum. Above this threshold, the growth rate varies as the third power of supersaturation and is hence controlled by the maximum speed of surface integration of new ions, inducing hopper growth as seen centrally in (Figure 7b). Rhombohedral growth is limited by the incorporation of ions into the calcite surface, with new surfaces being created in their place, where the position of the calcite likely limits ion availability due to the presence of the oil phase.[48] Both galena (cubic) and calcite (trigonal) are prone to hopper growth, indicating a degree of structural similarity that may prompt incorporation of PbS into the calcite structure during co-precipitation.[48, 50]

The exceedingly high initial supersaturation of PbS resulted in spontaneous precipitation of nanoparticles that acted as seeding points for the crystallization and growth of calcite by occlusion co-crystallisation.[37] Calcite is naturally hydrophilic, with a water contact angle of 6° and as such

would not typically adsorb at the o-w interface.[51] The occlusion of PbS agglomerates into the calcite structure enhanced hydrophobicity of the complex, leading to stronger interfacial adsorption. Andersson et al.[52] show that incorporation of the weakly hydrated lead ion into the calcite lattice through cation substitution leads to increased hydrophobicity of the calcite structure.

At pH values between approximately 4.6 and 8.9, where the pH of formation water lies, it is possible for sulfate groups to form on PbS, even when conditions are anoxic, due to the biological action of sulfide-oxidizing bacteria (SOB) that are commonly found in oilfield systems.[53-55] This will, as with sulfate rich organic sites within an eggshell membrane that promote calcification, create an area of elevated local supersaturation at the surface of the PbS agglomerate extending into the aqueous phase to which Ca^{2+} and CO_3^{2-} ions from solution migrate and nucleate.[56] It is possible that, due to high $SR_{Initial}$ of $CaCO_3$, flat amorphous calcium carbonate (ACC) aggregates accumulate on the PbS surface immersed within the aqueous solution, forming substantial deposits. The $CaCO_3$ mineral deposits then transform through secondary nucleation into large calcite crystals, with disk-shaped ACC and smaller $CaCO_3$ on the surface dissolving and supplying ions for further calcite growth where flat surfaced morphologies are dominant. The flower-shape of the calcite that occluded the PbS agglomerate at the interface is likely a result of the secondary nucleation determining the calcite orientation, based on the initial calcite seeds that provided a template for propagation of the initial ACC front transforming to calcite at neutral pH values (< 7). The presence of impurities such as Mg^{2+} ions has been shown to remove the intermediary transformation stage, where vaterite is formed as a pre-cursor to calcite under ambient conditions.[56, 57, 58] An illustration of this process as it potentially occurs in PbS and $CaCO_3$ multiphase scaling systems can be seen in Figure 9, where PbS agglomerates adsorbed at the o-w

interface are occluded within growing ACC that then transforms to large calcite crystals anchored

at the interface (a-d).
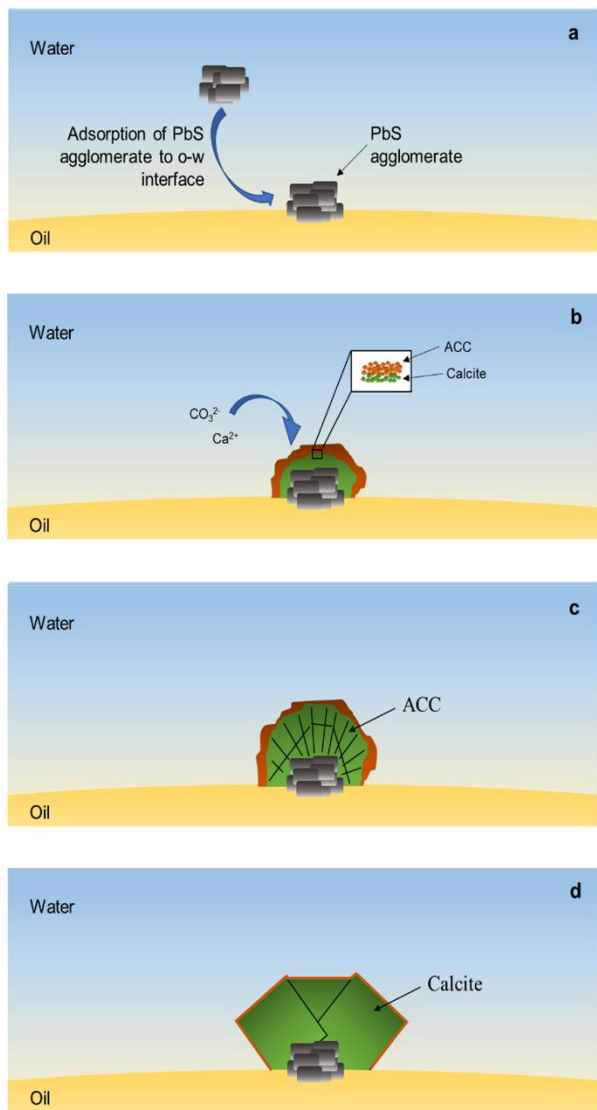
Figure 9 Growth of calcite around occluded PbS agglomerates at an o-w

interface (adapted from Navarro et al.) [53]

Pre-precipitation

experiments, whereby PbS nanoparticles were introduced into the reaction vessel prior to $CaCO_3$

precipitation displayed a similar scale formation to those co-precipitated, demonstrating that

agglomerates acted as seeding points at the o-w interface, where deposited PbS/calcite structures are similar to those seen in co-precipitation tests (Supporting Information Figure S4).

4.2. Scale deposition

4.2.1. Oil-in-water (o/w) emulsion

Figure 10a shows PbS deposition upon anti-fouling coupons in a multiphase system with an o:w ratio of 5:95, whereby PbS nanoparticle stabilized oil droplets have impacted fouled surfaces. F1 and F2 remain clear of scale, while REF and DLC showed heavy deposition. This can be attributed to the oil wetting characteristics of the hydrophobic coatings limiting interaction with the PbS scale containing aqueous phase. As a consequence of the high stability of Pickering emulsions, the structure of the stabilized droplet is still visible on the REF and DLC coupons, where oil droplet impaction did not lead to rupture.

Figure 10b shows PbS/CaCO$_3$ deposition upon anti-fouling coupons in a multiphase system with an o:w ratio of 5:95, leading to the formation of an o/w Pickering emulsion. It can be seen that far heavier deposition occurred on the REF and DLC surfaces, as opposed to the largely scale-free F1 and F2 hydrophobic coatings. After droplet impaction and rupture however, interfacially stabilized particles remained interlinked, maintaining a persistent film after deposition upon a surface as seen on the REF coupon. Crystal arrangement at the o-w interface can have a significant influence on emulsion stability, where attraction and bridging of particles leads to the formation of a rigid layer or 'shell', cocooning the droplet that forms a film upon rupture.[59, 60]

a REF F1 F2 DLC

b REF F2 F1 DLC
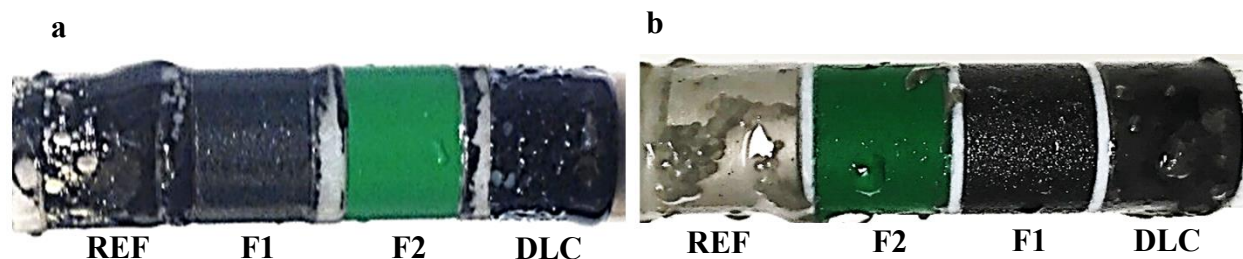
Figure 10 Anti-fouling coupons in a o/w multiphase system (5:95 o:w ratio) – a) PbS; b) PbS/$CaCO_3$ system

Impaction of the PbS particle-stabilized oil droplets appears from SEM images to occur via radial splashing, whereby a circular area of the DLC substrate is left relatively scale-free, with particles splashing and emanating outward after contact (Figure 11).
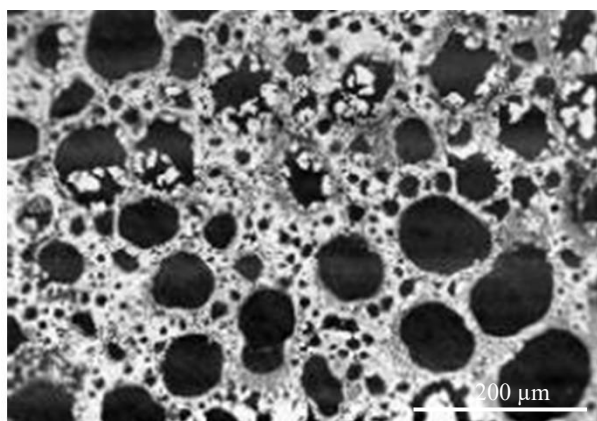
Figure 11 SEM of deposition pattern on DLC coupon

in a o/w multiphase PbS system (from Figure 10a)

Figure 12a and Figure 12b show SEM and EDX imaging on the REF coupon respectively, with the PbS/$CaCO_3$ complexes anchored and grown at the o-w interface depositing as flower-like structures recognizable from those observed from cryo-SEM analysis of the emulsion (Figure 7). Underlying heterogenous calcite deposits nucleated directly upon the surface may act as points of attachment for the homogenously deposited PbS/$CaCO_3$ complexes, where droplet rupture results in the radial splashing of co-precipitated particles upon hydrophilic surfaces.[28, 29] Bridging and interlocking of the arrangement of PbS/$CaCO_3$ complexes at the o-w interface (Figure 7) prompted

formation of a persistent film as described by Douaire et al.,[59] resulting in significant deposition after droplet impaction, best represented on the REF coupon in Figure 10b. EDX analysis further highlights the presence of incorporated PbS agglomerates (blue) within flower-shaped calcite structures (yellow/red).
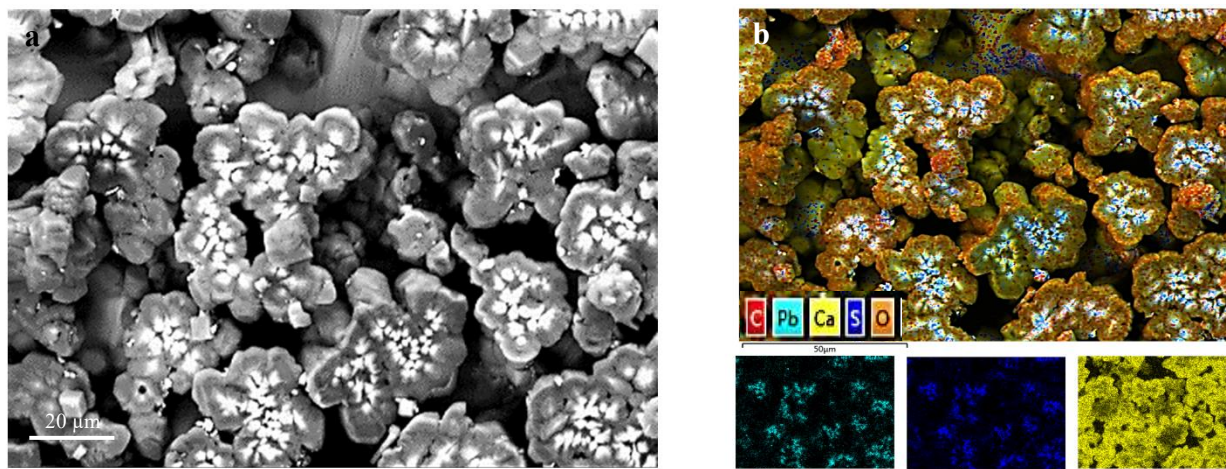
Figure 12 Deposited PbS/CaCO$_3$ complexes in o/w emulsion (REF coupon) – o:w 5:95 ratio; a) SEM; b) EDX

Figure 13a plots the coating water contact angle against the mass gain for a multiphase PbS system with an o:w ratio of 5:95. There was a reasonable correlation between wettability and mass deposited (R^2 = 0.79), where PbS fouling generally decreased with increasing surface hydrophobicity.

For PbS/CaCO$_3$, as with simple PbS based multiphase systems, there was a strong correlation between the water contact angle of the coating and the mass gain upon coatings (Figure 13b) due to the tendency of the oil phase to envelop hydrophobic surfaces where R^2 = 0.96. This is counter to simple CaCO$_3$ systems, where heterogeneous nucleation occurs upon both hydrophobic and hydrophilic surfaces, negating the correlation caused by envelopment of the oil layer around F1

and F2 to prevent deposition.[13] The recorded mass gain upon the surfaces of hydrophilic coupons was significantly higher than in simple PbS systems, likely due to the large size and hence mass of the calcite crystal, with deposits on the REF coupon weighing 0.32 mg/cm^2 and 3.77 mg/cm^2 for a PbS and PbS/CaCO$_3$ o/w system respectively.

a

Equation	y = a + b*x
Plot	Mass gain
Intercept	4.40971 ± 1.54476
Slope	-0.04201 ± 0.02148
R-Square (COD)	0.7927

b

Equation	y = a + b*x
Plot	Mass gain
Intercept	38.62855 ± 4.6765
Slope	-0.36597 ± 0.05358
R-Square (COD)	0.9589
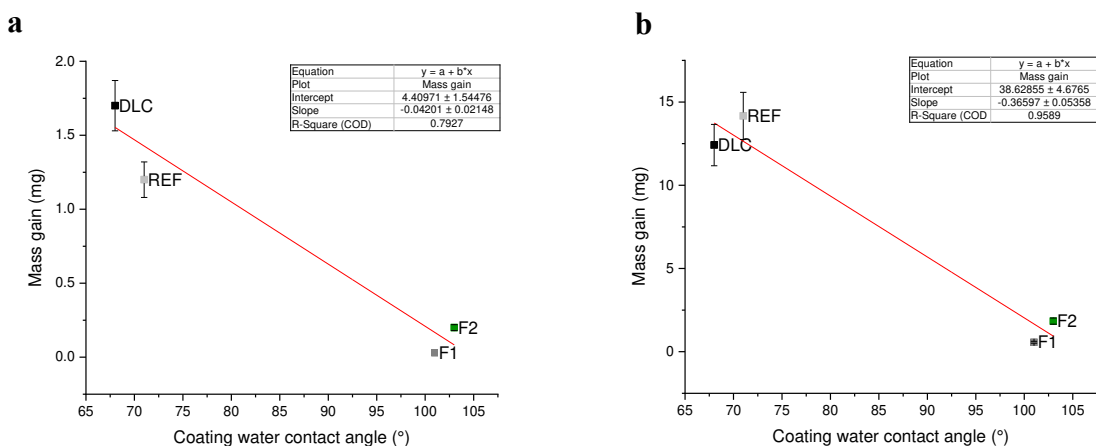
Figure 13 Water contact angle vs. mass gain with linear regression line; a) multiphase PbS system (o:w 5:95 ratio); b) multiphase PbS/CaCO$_3$ system (o:w 5:95 ratio)

4.2.2. Water-in-oil (w/o) emulsion

Figure 14a displays PbS deposition upon anti-fouling coupons in a multiphase system with an o:w ratio of 80:20, where high oil volume fraction lead to a w/o emulsion and PbS stabilized water droplets were the disperse phase. F1 and F2 remained clear of scale, while REF and DLC showed heavy deposition. Whilst excess oil present prevented fouling upon the hydrophobic fluoropolymer coatings, the low stability of the inverted emulsion lead to a high degree of surface deposition upon hydrophilic substrates. This can be likely explained by the ease with which the unstable water droplets rupture having impacted the surface, resulting in a clear lack of persistent droplets, unlike those seen in Figure 10a upon the REF coupon.

PbS/CaCO$_3$ deposition upon anti-fouling coupons in a w/o emulsion, where o:w ratio is 60:40, can be seen in Figure 14b. As with scaling in the o/w emulsion system, hydrophobic fluoropolymers F1 and F2 are scale-free, whilst the hydrophilic REF and DLC have a significant amount of deposition upon their surface. Excess oil, readily available to envelop the hydrophobic surfaces, prevents the deposition of PbS/CaCO$_3$ stabilized emulsion that is prone to impaction on surfaces contained within the aqueous phase.
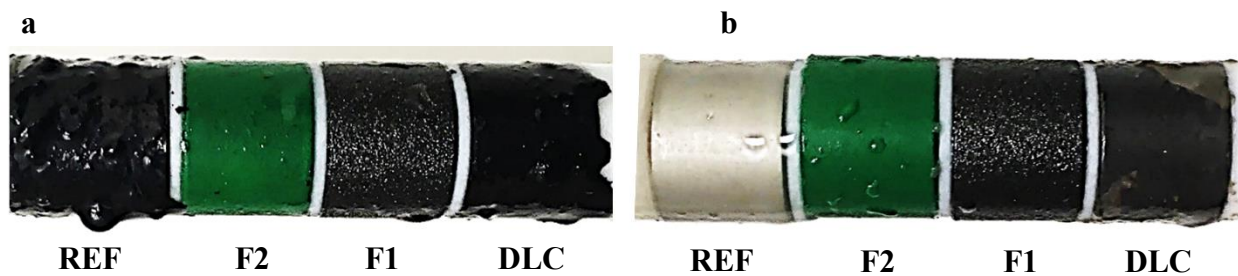
Figure 14 Anti-fouling coupons in a w/o multiphase system (80:20 o:w ratio) – a) PbS; b) PbS/CaCO$_3$ system

SEM imaging of the surface of REF and DLC coupons in w/o emulsion PbS systems revealed uniform and 100% coverage. SEM and EDX imaging of the REF coupon in PbS/CaCO$_3$ systems (Figure 15) revealed the familiar pattern whereby PbS agglomerates acted as seeds for calcite nucleation and growth before deposition through emulsion droplet impaction upon the REF coupon. The average size of the PbS/CaCO$_3$ complexes varied from 10-20 µm, smaller than in o/w systems where typical size of PbS/CaCO$_3$ complexes ranged from 20-30 µm. Reduction in the availability of scaling ions due to a reduction in overall aqueous volume (0.95 to 0.4 volume fraction) was likely responsible for the limited growth of calcite structures around PbS agglomerate clusters.
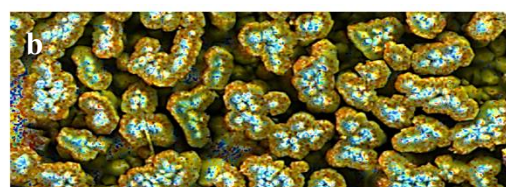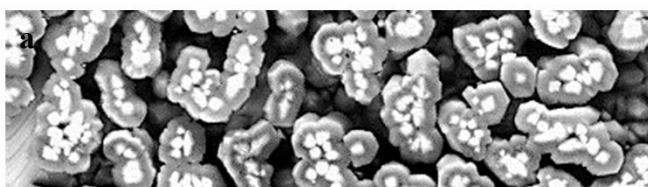
Figure 15 Deposited PbS/CaCO$_3$ complexes in w/o emulsion (REF coupon) – o:w 80:20 ratio; a) SEM; b) EDX

Figure 16a plots the coating water contact angle against the mass gain for a multiphase PbS system with an o:w ratio of 80:20. As with o/w emulsion scaling in Figure 16a, there was a strong correlation between coating wettability and mass deposited ($R^2 = 0.79$), with PbS fouling generally decreasing with increasing surface hydrophobicity.

Figure 16b showed that similarly to deposition in o/w PbS/CaCO$_3$ Pickering emulsion systems, hydrophilic coatings saw a proportionally high degree of mass gain due to the lack of an enveloping oil layer on the surface, whereas hydrophobic fluoropolymers F1 and F2 received less than 0.27 mg/cm^2 of scaling where $R^2 = 0.47$. Whilst the correlation appeared weak due to limited deposition upon the REF coupon, it was still apparent that surface hydrophobicity played a significant role in reducing deposition in PbS/CaCO$_3$ w/o systems.

a

Equation	y = a + b*x
Plot	Mass gain
Intercept	10.50932 ± 3.17685
Slope	-0.10058 ± 0.0364
R-Square (COD	0.79247

b

Equation	y = a + b*x
Plot	Mass gain
Intercept	49.92539 ± 27.635
Slope	-0.51771 ± 0.3908
R-Square (COD	0.46737

27
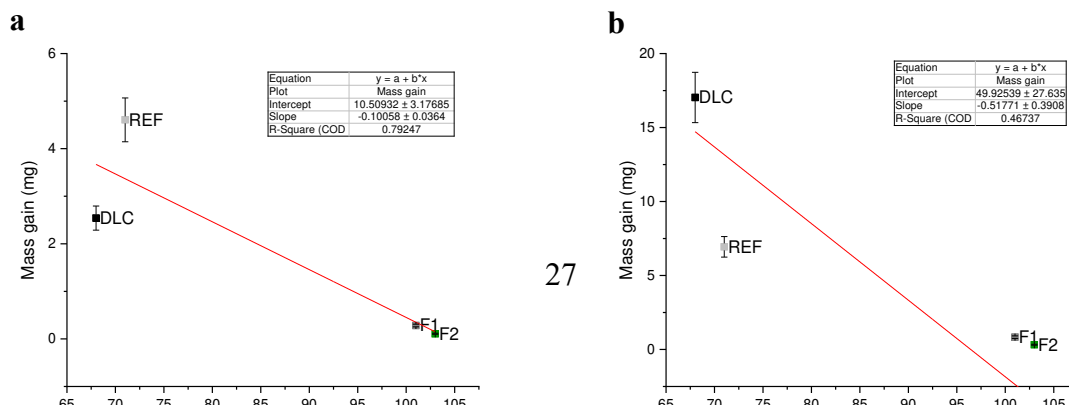
Figure 16 Water contact angle vs. mass gain with linear regression line; a) multiphase PbS system (o:w 80:20 ratio); b) multiphase PbS/CaCO₃ system (o:w 60:40 ratio)

5. Conclusion

Determination of galena wettability through inverted sessile drop measurements at a galena-oil-water interface, where oil contact angle on a galena surface was $132.1 \pm 0.8°$, demonstrated the partial hydrophobicity of PbS particles and explained their tendency to assemble at the aqueous boundary of the droplet interface in an emulsion, as shown by cryo-SEM analysis. As was predicted for hydrophilic particles forming Pickering emulsions, o/w type was the favored emulsion state, where catastrophic inversion to w/o only occurred when oil phase fraction was above 0.75. It was demonstrated during depositional experiments on surfaces of different wettability in a turbulent multiphase, simple PbS scaling system that inversion of the emulsion had no effect on the trend observed in which substrates with a higher degree of hydrophobicity see a lower proportion of PbS deposition.

The mechanism of PbS deposition has been shown to occur as a result of transportation at the o-w interface of the dispersed phase of an emulsion, before impacting a surface and adhering. Whilst previous studies by Keogh et al.[4, 13] have shown that PbS deposition is negligible on hydrophobic surfaces in an o/w emulsion, the influence on deposition of a low-water cut w/o emulsion had not

been investigated. The results herein show that hydrophobic surfaces were indeed able to virtually negate PbS deposition in a w/o system due to the oil-wetting effect upon their surface.

CaCO$_3$ deposition is extensive on surfaces of all wettability in simple CaCO$_3$ multiphase scaling systems, a consequence of heterogeneous nucleation that compromises the anti-fouling characteristics and prompts localized scale deposition and build-up.[13] The introduction of PbS nanoparticles to an identical system provides a seeding point and an energetically favorable pathway to nucleation, prompting heterogeneous growth at the o-w interface as seen in Figure 7.[61] Allowing the interfacial growth of scaling minerals through the use of seeding techniques, the stabilizing particles of which favor the aqueous phase, may be a valid means of averting the initial nucleation and deposition of scale upon hydrophobic anti-fouling surfaces in oilfield systems. Co-precipitation of PbS and CaCO$_3$ in a turbulent multiphase system resulted in the formation of a Pickering emulsion. PbS agglomerates were occluded into a flower-shaped calcite structure that stabilized droplets at the o-w interface within the emulsion, with ACC predicted to act as a precursor to the secondary nucleation of large calcite crystals. Spontaneous nucleation of PbS in the bulk aqueous phase as a result of an exceedingly high SR$_{initial}$, resulted in adsorption of particles and agglomerates to the o-w interface that then acted as seeding points for the secondary nucleation of slow growing calcite structures. Though not investigated in this work, it is feasible that the high SR$_{initial}$ of other minerals prone to precipitating in oilfield systems e.g. ZnS and FeS, could also result in occlusion within calcite structures and the formation of complexes.

Emulsion type was inverted from o/w to w/o at approximately > 0.5 oil volume fraction, indicating that bridging and ripening of dispersed droplets stabilized by PbS/CaCO$_3$ complexes occurred more readily than in simple PbS systems due to lower neat packing fraction at the o-w

interface. In both PbS and PbS/CaCO$_3$ scaling systems, depositional tendency remained similar, where the presence of oil at a low phase fraction of 0.05 in o/w systems was sufficient to prevent scaling upon hydrophobic surfaces. Consequently, phase inversion in multiphase systems is unlikely to have a significant impact on scale deposition and build-up in producing oilfield wells, with w/o emulsion systems showing marginally more scale build-up on hydrophilic substrates. Topside processes such as oil/water separation may be influenced by the specific phase inversion ratio of different solid stabilized emulsions, with hydrocyclones reported to show a reduction in efficiency around the region of catastrophic phase inversion.[62]

Associated Content

Supporting information

Solution composition (Table S1)

Proportion of solution mixed to form acetate buffer (Table S2)

Cell for inverted sessile drop measurements (Figure S1)

Pre-precipitation of PbS in PbS/CaCO$_3$ systems (Figure S2)

Oil (in solution) and water (in air) contact angles on cleaved galena (Figure S3)

XRD spectra of PbS/CaCO$_3$ stabilized emulsion (Figure S4)

Author Information

Corresponding Author

*Phone: +447772076496. E-mail: pm09wk@leeds.ac.uk.

ORCID

William Keogh:0000-0003-3676-8129

Nomenclature

ACC = amorphous calcium carbonate

BSE = backscattered electron

$CaCO_3$ = calcium carbonate

EDL = electrostatic double layer

EDX = energy-dispersive X-ray spectroscopy

FeS = iron sulfide

FW = formation water

H_2S = hydrogen sulfide

HT/HP = high temperature/high pressure

IAP = ion activity product

k_bT = energy (J)

KCl = potassium chloride

K_{sp} = solubility product

N$_2$ = nitrogen

NaCl = sodium chloride

o/w = oil in water emulsion

PbS = lead sulfide

SEM = scanning electron microscopy

SOB = Sulfide Oxidizing Bacteria

SR = saturation ratio

SW = seawater

TDS = total dissolved solids

TEM = transmission electron microscopy

vdW = van der Waals

w/o = water in oil emulsion

XRD = X-ray diffraction

ZnS = zinc sulfide

ζ = zeta potential

References

1.   Crabtree, M.; Eslinger, D.; Fletcher, P.; Miller, M.; Johnson, A.; King, G., Fighting scale—removal and prevention. *Oilfield Review* **1999,** 11, (3), 30-45.
2.   Kelland, M. A., *Production Chemicals for the Oil and Gas Industry, Second Edition*. Taylor & Francis: 2014.
3.   Jordan, M.; Mackin, K.; Johnston, C.; Feasey, N. In *Control of hydrogen sulphide scavenger induced scale and the associated challenge of sulphide scale formation within a North Sea high temperature/high salinity fields production wells. Laboratory evaluation to field application*, SPE International Symposium on Oilfield Scale, 2004; Society of Petroleum Engineers: 2004.
4.   Keogh, W.; Charpentier, T.; Neville, A.; O'Brien, A.; Eroini, V.; Olsen, J. H.; Nielsen, F. M.; Ellingsen, J. A.; Bache, O.; Baraka-Lokmane, S., Evaluation of Anti-Fouling Surfaces for Prevention of Lead Sulfide Scaling in Single and Multiphase Conditions. In *CORROSION 2017*, NACE International: New Orleans, Louisiana, USA, 2017; p 15.
5.   Zarga, Y.; Boubaker, H. B.; Ghaffour, N.; Elfil, H. J. C. E. S., Study of calcium carbonate and sulfate co-precipitation. **2013,** 96, 33-41.
6.   Sheikholeslami, R.; Ng, M. J. I.; research, e. c., Calcium sulfate precipitation in the presence of nondominant calcium carbonate: thermodynamics and kinetics. **2001,** 40, (16), 3570-3578.

7.   Chen, T.; Neville, A.; Yuan, M., Calcium carbonate scale formation—assessing the initial stages of precipitation and deposition. *Journal of Petroleum Science and Engineering* **2005,** 46, (3), 185-194.

8.   Clever, H. L.; Johnston, F. J., The solubility of some sparingly soluble lead salts: an evaluation of the solubility in water and aqueous electrolyte solution. *Journal of Physical and Chemical Reference Data* **1980,** 9, (3), 751-784.

9.   Frota, T.; Silva, D.; Aguiar, J.; Anjos, R.; Silva, I. J. B. J. o. P.; Gas, Assessment of scale formation in the column of an oil and natural gas producing well: A case study. **2013,** 7, (1).

10.   Baraka-Lokmane, S.; Hurtevent, C.; Zhou, H.; Saha, P.; Tots, N.; Rieu, F.; Lastennet, R.; Sugiarto, T. In *TOTAL's Experience on the Development and Implementation of a Scale Management Strategy in Central Graben Fields*, SPE International Oilfield Scale Conference and Exhibition, 2014; Society of Petroleum Engineers: 2014.

11.   Okocha, C.; Sorbie, K. In *Scale Prediction for Iron, Zinc and Lead Sulphides and Its Relation to Scale Test Design*, CORROSION 2014, 2014; NACE International: 2014.

12.   Al-Harbi, B. G.; Graham, A. J.; Sorbie, K. S., Zinc and Lead Interactions in Combined Sulphide Scales. In Society of Petroleum Engineers.

13.   Keogh, W.; Neville, A.; Huggan, M.; Eroini, V.; Olsen, J. H.; Nielsen, F. M.; Baraka-Lokmane, S.; Bourdelet, E.; Ellingsen, J. A.; Bache, O. J. E.; Fuels, Deposition of Inorganic Carbonate, Sulfate, and Sulfide Scales on Antifouling Surfaces in Multiphase Flow. **2017,** 31, (11), 11838-11851.

14.   Scanlon, B. R.; Reedy, R. C.; Male, F.; Walsh, M. J. E. s.; technology, Water issues related to transitioning from conventional to unconventional oil production in the Permian Basin. **2017,** 51, (18), 10903-10912.

15.   Binks, B. P.; Lumsdon, S. J. L., Influence of particle wettability on the type and stability of surfactant-free emulsions. **2000,** 16, (23), 8622-8631.

16.   Lewis, A. E. J. H., Review of metal sulphide precipitation. **2010,** 104, (2), 222-234.

17.   Reed, M. H.; Palandri, J. J. R. i. M.; Geochemistry, Sulfide mineral precipitation from hydrothermal fluids. **2006,** 61, (1), 609-631.

18.   Barrett, T.; Anderson, G. J. G. e. C. A., The solubility of sphalerite and galena in 1–5 m NaCl solutions to 300 C. **1988,** 52, (4), 813-820.

19.   Keogh, W.; Boakye, G. O.; Neville, A.; Charpentier, T.; Olsen, J. H.; Eroini, V.; Nielsen, F.; Ellingsen, J.; Bache, O.; Baraka-Lokmane, S. In *Lead Sulfide (PbS) Scale Behavior and Deposition as a Function of Polymeric Sulfide Inhibitor Concentration in Multiphase*, NACE 2018: Proceedings of the International Corrosion Conference and Expo Series, 2018; National Association of Corrosion Engineers: 2018.

20.   Polte, J. J. C., Fundamental growth principles of colloidal metal nanoparticles–a new perspective. **2015,** 17, (36), 6809-6830.

21.   Söhnel, O.; Mullin, J., Precipitation of calcium carbonate. *Journal of Crystal Growth* **1982,** 60, (2), 239-250.

22.   MacAndrew, R. J. J. o. P. T., Technology Focus: HP/HT Challenges (April 2008). **2008,** 60, (04), 88-88.

23.   Vu, H. P.; Black, J. R.; Haese, R. R. J. E. P., Changes in formation water composition during water storage at surface and post re-injection. **2017,** 114, 5732-5741.

24.   Nehrke, G.; Reichart, G.-J.; Van Cappellen, P.; Meile, C.; Bijma, J. J. G. e. C. A., Dependence of calcite growth rate and Sr partitioning on solution stoichiometry: non-Kossel crystal growth. **2007,** 71, (9), 2240-2249.

25.   Khodakarami, M.; Alagha, L.; Burnett, D. J., Probing Surface Characteristics of Rare Earth Minerals Using Contact Angle Measurements, Atomic Force Microscopy, and Inverse Gas Chromatography. *ACS omega* **2019,** 4, (8), 13319-13329.

26.   Nonomura, Y.; Kobayashi, N. J. J. o. c.; science, i., Phase inversion of the Pickering emulsions stabilized by plate-shaped clay particles. **2009,** 330, (2), 463-466.

27.   Chen, J.; Long, X.; Chen, Y., Comparison of Multilayer Water Adsorption on the Hydrophobic Galena (PbS) and Hydrophilic Pyrite (FeS2) Surfaces: A DFT Study. *The Journal of Physical Chemistry C* **2014,** 118, (22), 11657-11665.

28.   Ok, H.; Park, H.; Carr, W. W.; Morris, J. F.; Zhu, J. J. J. o. d. s.; technology, Particle-Laden Drop Impacting on Solid Surfaces. **2005,** 25, (4), 449-456.

29.   Grishaev, V.; Iorio, C. S.; Dubois, F.; Amirfazli, A. J. L., Complex drop impact morphology. **2015,** 31, (36), 9833-9844.

30.   Jarzabek, D. M.; Chmielewski, M.; Dulnik, J.; Strojny-Nedza, A. J. J. o. M. E.; Performance, The influence of the particle size on the adhesion between ceramic particles and metal matrix in MMC composites. **2016,** 25, (8), 3139-3145.

31.   Leite, F. L.; Bueno, C. C.; Da Róz, A. L.; Ziemath, E. C.; Oliveira, O. N. J. I. j. o. m. s., Theoretical models for surface forces and adhesion and their measurement using atomic force microscopy. **2012,** 13, (10), 12773-12856.

32.   Sudmalis, M.; Sheikholeslami, R., Coprecipitation of CaCO3 and CaSO4. *The Canadian Journal of Chemical Engineering* **2000,** 78, (1), 21-31.

33.   Zarga, Y.; Boubaker, H. B.; Ghaffour, N.; Elfil, H., Study of calcium carbonate and sulfate co-precipitation. *Chemical Engineering Science* **2013,** 96, 33-41.

34.   Dunitz, J. D. J. C., Crystal and co-crystal: a second opinion. **2003,** 5, (91), 506-506.

35.   Kumagai, T. J. R., Coprecipitation of cadmium with calcium carbonate from aqueous solutions at 15 to 50℃. **1992,** 41, 57-63.

36.   Bard, A. J.; Inzelt, G.; Scholz, F., *Electrochemical dictionary*. Springer Science & Business Media: 2008.

37.   Mallampati, R.; Valiyaveettil, S. J. R. A., Co-precipitation with calcium carbonate–a fast and nontoxic method for removal of nanopollutants from water? **2015,** 5, (15), 11023-11028.

38.   Li, S.-S.; Chang, C.-H.; Wang, Y.-C.; Lin, C.-W.; Wang, D.-Y.; Lin, J.-C.; Chen, C.-C.; Sheu, H.-S.; Chia, H.-C.; Wu, W.-R. J. E.; Science, E., Intermixing-seeded growth for high-performance planar heterojunction perovskite solar cells assisted by precursor-capped nanoparticles. **2016,** 9, (4), 1282-1289.

39.   Baraka-Lokmane, S.; Hurtevent, C.; Rossiter, M.; Bryce, F.; Lepoivre, F.; Marais, A.; Tillement, O.; Simpson, C.; Graham, G. In *Design and Performance of Novel Sulphide Nanoparticle Scale Inhibitors for North Sea HP/HT Fields*, SPE International Oilfield Scale Conference and Exhibition, 2016; Society of Petroleum Engineers: 2016.

40.   Kielland, J. J. J. o. t. A. C. S., Individual activity coefficients of ions in aqueous solutions. **1937,** 59, (9), 1675-1678.

41.   Kong, Y.; Chen, J.; Fang, H.; Heath, G.; Wo, Y.; Wang, W.; Li, Y.; Guo, Y.; Evans, S. D.; Chen, S. J. C. o. M., Highly fluorescent ribonuclease-A-encapsulated lead sulfide quantum dots for ultrasensitive fluorescence in vivo imaging in the second near-infrared window. **2016,** 28, (9), 3041-3050.

42.   Mullin, J. W., *Crystallization*. Butterworth-Heinemann: 2001.

43.   Binks, B.; Lumsdon, S., Catastrophic phase inversion of water-in-oil emulsions stabilized by hydrophobic silica. *Langmuir* **2000,** 16, (6), 2539-2547.

44.   Manocha, A.; Park, R. L. J. A. o. S. S., Flotation related ESCA studies on PbS surfaces. **1977,** 1, (1), 129-141.

45.   Whitby, C.; Wanless, E., Controlling Pickering emulsion destabilisation: A route to fabricating new materials by phase inversion. *Materials* **2016,** 9, (8), 626.

46.   Cates, M. J. S. I. L. N. o. t. L. H. S. S. V., July, Complex fluids: the physics of emulsions. **2017,** 98, 317.

47.   Whitby, C. P.; Wanless, E. J., Controlling Pickering Emulsion Destabilisation: A Route to Fabricating New Materials by Phase Inversion. *Materials (Basel, Switzerland)* **2016,** 9, (8), 626.

48. Desarnaud, J.; Derluyn, H.; Carmeliet, J.; Bonn, D.; Shahidzadeh, N. J. T. j. o. p. c. l., Hopper Growth of Salt Crystals. **2018**.

49. Ritchie, A. W.; Watson, M. I.; Turnbull, R.; Lu, Z. Z.; Telfer, M.; Gano, J. E.; Self, K.; Greer, H. F.; Zhou, W. J. C., Reversed crystal growth of rhombohedral calcite in the presence of chitosan and gum arabic. **2013,** 15, (47), 10266-10271.

50. Bonev, I. K.; Rice, C. M. J. M. M., Single crystal galena pillars as highly anisometric dissolution forms. **1997,** 61, (3), 377-386.

51. Kowalczuk, P. B.; Akkaya, C.; Ergun, M.; Janicki, M.; Sahbaz, O.; Drzymala, J. J. P. P. o. M. P., Water contact angle on corresponding surfaces of freshly fractured fluorite, calcite and mica. **2017,** 53.

52. Andersson, M. P.; Dideriksen, K.; Sakuma, H.; Stipp, S. L. S. J. S. r., Modelling how incorporation of divalent cations affects calcite wettability–implications for biomineralisation and oil recovery. **2016,** 6, 28854.

53. De Giudici, G.; Ricci, P.; Lattanzi, P.; Anedda, A., Dissolution of the (001) surface of galena: An in situ assessment of surface speciation by fluid-cell micro-Raman spectroscopy. *American Mineralogist* **2007,** 92, (4), 518-524.

54. Jenneman, G. E.; Gevertz, D. In *Identification, characterization and application of sulfide-oxidizing bacteria in oil fields*, Proceedings of the 8th International Meeting on Microbial Ecology, Halifax, Nova Scotia, 1999; 1999.

55. Schippers, A., Biogeochemistry of metal sulfide oxidation in mining environments, sediments, and soils. *Special Papers-Geological Society Of America* **2004**, 49-62.

56. Rodríguez-Navarro, A. B.; Marie, P.; Nys, Y.; Hincke, M. T.; Gautron, J., Amorphous calcium carbonate controls avian eggshell mineralization: a new paradigm for understanding rapid eggshell calcification. *Journal of structural biology* **2015,** 190, (3), 291-303.

57. Addadi, L.; Moradian, J.; Shay, E.; Maroudas, N. G.; Weiner, S., A chemical model for the cooperation of sulfates and carboxylates in calcite crystal nucleation: Relevance to biomineralization. **1987,** 84, (9), 2732-2736.

58. Rodriguez-Blanco, J.; Shaw, S.; Bots, P.; Roncal-Herrero, T.; Benning, L., The role of pH and Mg on the stability and crystallization of amorphous calcium carbonate. *Journal of Alloys and Compounds* **2012,** 536, S477-S479.

59. Douaire, M.; Di Bari, V.; Norton, J.; Sullo, A.; Lillford, P.; Norton, I. J. A. i. c.; science, i., Fat crystallisation at oil–water interfaces. **2014,** 203, 1-10.

60. Chacon, L.; Baret, J. J. J. o. P. D. A. P., Microfluidic angle of repose test for Pickering emulsions. **2017,** 50, (39), 39LT04.

61. Binsbergen, F. J. P. i. s. s. c., Heterogeneous nucleation of crystallization. **1973,** 8, 189-238.

62. Belaidi, A.; Thew, M. T.; Munaweera, S. J., Hydrocyclone Performance with Complex Oil-Water Emulsions in the Feed. *The Canadian Journal of Chemical Engineering* **2003,** 81, (6), 1159-1170.